ISPRS Journal of Photogrammetry and Remote Sensing 148 (2019) 174–183

Contents lists available at ScienceDirect

ISPRS Journal of Photogrammetry and Remote Sensing

journal homepage: www.elsevier.com/locate/isprsjprs

TanDEM-X digital surface models in boreal forest above-ground biomass change detection

Kirsi Karila[a,*], Xiaowei Yu[a], Mikko Vastaranta[b], Mika Karjalainen[a], Eetu Puttonen[a], Juha Hyyppä[a]

[a] Finnish Geospatial Research Institute (FGI) at the National Land Survey of Finland, Geodeetinrinne 2, 02431 Masala, Finland
[b] School of Forest Sciences, University of Eastern Finland, P.O. Box 111, 80101 Joensuu, Finland

ARTICLE INFO

Keywords:
Tandem-X
SAR interferometry
Above-ground biomass (AGB)
Forest
Airborne laser scanning (ALS)
LIDAR
Change detection

ABSTRACT

Satellite images provide spatially explicit information on forest change covering wide areas. In this study, bistatic TanDEM-X (TDX) synthetic aperture radar (SAR) satellite data were used to derive digital surface models (DSMs) of forest areas using SAR interferometry (InSAR). The capability of change features derived from bi-temporal InSAR DSMs to detect forest height (90th percentile of canopy height distribution, H90) and density variations was investigated. Moreover, changes in the forest above-ground biomass (AGB) were estimated from height changes between two InSAR DSMs. Bi-temporal airborne laser scanning (ALS) data, aerial orthoimages and an ALS-based AGB change map from a study area in Southern Finland were used as references. The results indicate that the InSAR height change of a forested area correlates more with vegetation density change than with height change. The correlation between the InSAR mean height change and the height change feature from ALS was 0.76 at stand level. Correspondingly, the correlation between the InSAR mean height change and the ALS penetration rate change was 0.89. The AGB changes predicted based on InSAR height change agreed well with the reference data; the root-mean-square error (RMSE) was 20.7 Mg/ha (18.5% of the mean biomass in 2012) at stand level and 27.4 Mg/ha (27.0%) for 16 × 16 m grid cells. The results show that TDX DSMs can be used to detect biomass changes of different orders of magnitude, e.g. due to logging and thinning.

1. Introduction

Planning sustainable use of forests and carbon monitoring require up-to-date estimates of forest biomass. In addition, biomass estimates may be required for areas outside of the typically inventoried land-base (i.e. non-merchantable or remote locations) or out of sync with existing inventory cycles. As such, in addition to typically used airborne images or laser scanning (ALS) data, supplementary remote sensing data are needed to capture biomass and biomass change. Satellite images can be used to cover large areas of forest with consistent data in a cost-effective way (Lunetta et al., 2004).

One of the most important forest-related parameters is above-ground biomass (AGB) and its changes, which are also known to have an effect on the global carbon cycle (Houghton, 2005; Bonan, 2008). Remote sensing provides spatially explicit information about forests that could in future be integrated into greenhouse gas reporting systems (Boisvenue et al., 2016). The value of the carbon mitigated by forests could be billions of euros annually based on current European emission allowances (Eurostat, 2018; EEX, 2018). However, there is uncertainty in the current carbon exchange models (Bradshaw and Warkentin, 2015). Thus, small improvements in modeling could be worth millions of euros.

Forest maps covering large areas can be derived from optical satellite imagery (e.g. Hansen et al., 2013; Hermosilla et al., 2015) and synthetic aperture radar (SAR) satellite imagery (Wagner et al., 2003; Persson et al., 2017). Forest AGB is often mapped using medium-resolution satellite imagery (Song, 2012), for example from Landsat and Sentinel satellites, which provide open-access data acquired several times per year and covering wide areas (Drusch et al.,2012; Wulder et al., 2012).

Recently, satellite systems capable of extracting elevation models (3D features) have been found to be a potential remote sensing data source for forest AGB mapping (St-Onge et al., 2008; Solberg et al., 2010; Persson et al., 2013). Very-high-resolution (VHR) satellite imagery can be used to extract forest canopy height models and furthermore to estimate AGB in more detail than the medium-resolution datasets. For example, high accuracy in biomass estimation from VHR satellite imagery has been achieved from Worldview-2 (Yu et al., 2015) and Pleaides (Persson, 2016) VHR optical stereo satellite imagery. However, the availability of suitable image pairs is limited due to cloud

* Corresponding author.
E-mail address: kirsi.karila@nls.fi (K. Karila).

https://doi.org/10.1016/j.isprsjprs.2019.01.002
Received 16 May 2018; Received in revised form 12 November 2018; Accepted 3 January 2019

coverage, and the coverage of VHR optical stereo images is somewhat limited compared to systems such as Landsat and Sentinel-2. In addition, the costs of VHR imagery are a limiting factor, although taking into account the recent developments in opening (open-access) data, the situation may change in the future.

When elevation models are extracted from SAR satellite data, the problems of cloud coverage can be omitted. From current operational satellite SAR systems, the highest biomass estimation accuracy has been achieved using Tandem-X interferometric image pairs (Askne et al., 2013; Yu et al., 2015). Tandem-X (TDX) is a system of two X-band SAR satellites flying in close formation (Krieger et al., 2007). The system enables bistatic image acquisition simultaneously using the two satellites. SAR interferometry (InSAR) (Bamler and Hartl, 1998) is a technique for generating a digital surface model (DSM) from two complex SAR images. Simultaneous acquisition increases the correlation between the SAR measurements, resulting in more accurate height estimates.

Relationship between forest height and C-band spaceborne SAR interferometric height was first analysed by Hagberg et al. (1995), and first models between InSAR and forest attributes in boreal forest were developed by Askne et al. (1997). For forested areas, interferometric height is different from the actual height of the canopy, and it depends on forest type and signal penetration into the canopy. Effects of forest type and SAR system frequency have been studied by Sarabandi and Lin (2000). For the X-band spaceborne SAR observations the height of the scattering phase center has been analyzed by Praks et al. (2012) and Kugler et al. (2014). Interferometric height and AGB are both related to forest canopy height and density (Treuhaft and Siqueira, 2004).

Estimating forest inventory attributes from Tandem-X data in boreal forests has been proven feasible in several studies; forest AGB has been derived from forest height using equations adopted for the target area and the forest type (Mette et al., 2003; Askne and Santoro, 2015; Torano et al., 2016; Askne et al., 2017, 2018), or by developing prediction models between the Tandem-X height metrics and AGB using in situ measurements from sample plots (Askne et al., 2013; Solberg et al., 2013a; Hansen et al., 2015; Karila et al., 2015; Soja et al., 2015a; Yu et al., 2015; Persson and Fransson, 2017; Persson et al., 2017).

Although it has been shown that the 3D features based on TDX do not describe the forest structure at plot level as accurately as ALS or optical imagery, the 3D features based on TDX correlate with the forest height and can be used consequently in the prediction of forest structural attributes – even at plot-level – with reasonable accuracy (Yu et al., 2015). It should be noted that due to the higher ground sampling distances and different measurement principles, TDX point clouds cannot be expected to capture the variation in forest height and canopy cover density in as detailed a manner as ALS. In addition, the method of deriving a point cloud from radar data affects the prediction accuracy: estimates for forest attributes based on TDX interferometry are consistently more accurate than estimates based on TerraSAR-X radargrammetry (Yu et al., 2015).

Although the potential of AGB mapping from bistatic interferometric SAR (InSAR) data is well known, there are still few scientific studies about the possibilities and accuracy to estimate AGB change from InSAR data. In previous studies, Tandem-X datasets have been used to detect biomass changes in tropical forests (Solberg et al., 2017; Treuhaft et al., 2017; Knapp et al., 2018). Change detection between interferometric data from the 30 m resolution SRTM (Shuttle Radar Topography Mission) data and TDX has been carried out in boreal forest by Solberg et al. (2014) and Næsset et al. (2015). These datasets have also been used to detect forest clear-cuts (Solberg et al., 2013b). In addition, change detection between ALS and TDX has been presented in Askne et al. (2017) and Tian et al. (2017). Detection of thinning and clear-cuts in boreal forest from solely TDX data was demonstrated by Persson et al. (2015). Detection of growth from TDX data has been recently studied by Askne et al. (2018).

This paper aims to improve the understanding of the feasibility of bi-temporal TDX DSMs to monitor forest AGB changes. The main strength of our study is the comprehensive reference data. We have forest field plots and accurate AGB reference maps based on bi-temporal ALS data. ALS point clouds accurately describe forest height, forest height variation and canopy cover. All of these factors correlate with forest AGB (e.g. Koch, 2010; Kaasalainen et al., 2014). Accurate estimates of forest inventory attributes have been provided by ALS (Næsset, 2007; Hyyppä et al., 2008; Kankare et al., 2013; Bouvier et al., 2015; Sheridan et al., 2015). ALS has also been proved to be a reliable method to monitor changes in vegetation height and density (Yu et al., 2008; Næsset et al., 2013; Vastaranta et al., 2013), and AGB changes have been accurately estimated from ALS (Økseter et al., 2015; Cao et al., 2016).

In order to monitor AGB, it is necessary to estimate changes in forest height and density due to forest growth, forest damage and forest management. Thus, in order to investigate the capability of the TDX data to characterize forest AGB changes, we investigated how reliably we can detect changes in forest height (90th percentile of canopy height distribution from ALS), and canopy cover (ALS penetration rate) from TDX DSMs. The relationship between interferometric height change and forest AGB change for a boreal forest study area in Southern Finland was also investigated.

2. Materials and methods

2.1. Study area and data

The study area is located in the southern boreal forest zone in Evo, Finland (61.19°N, 25.11°E). The size of the area is approximately 4200 ha. There are both managed and natural forest stands in the area. The most common tree species in the area are Scots pine (*Pinus sylvestris*, 40% of total volume) and Norway spruce (*Picea abies*, 35%). Deciduous trees comprise 24% of the total volume.

ALS data from the study area was acquired in summer 2012 and 2014. In both years, the area was covered by two scans. The 2012 dataset was acquired on May 7 and 13, 2012, using Optech ALTM Gemini and Leica ALS50 sensors. The flight altitudes were 1830 and 2200 m above ground level (AGL). The pulse density was 0.8 pulses per m^2. The data is an open dataset from the National Land Survey (NLS) of Finland. The 2014 ALS dataset was acquired on May 22 and September 8, 2014, using a Leica ALS70-HA SN 7202 sensor. The flying altitude was 2500 m AGL and the pulse density 0.7 pulses per m^2.

Field data was collected in 2014 for 91 sample plots of 32 by 32 m, which were further divided into 364 plots of 16 by 16 m (Yu et al., 2015). The sample plot level AGB was obtained by summing single tree level AGB's. The AGB for each single tree within a sample plot was calculated using a field-measured tree height, diameter at breast height (DBH) and tree species as inputs for a national biomass equation (Repola, 2008, 2009). The AGB (Mg/ha) estimate of the sample plot was derived from the absolute AGB by taking the plot size into account. For the sample plots, the minimum AGB was 19.1 Mg/ha, the maximum AGB 230.6 Mg/ha, and the mean AGB 134.5 Mg/ha; the standard deviation of AGB was 48.3 Mg/ha. No forest operations were carried out between 2012 and 2014 within the sample plots. Thus, the only change between 2012 and 2014 was growth, which is expected to be approximately 1.8 Mg/ha/year, based on forest growth simulations using field data. Thus, it has only a minor effect on the quality of our sample plot data between the two time periods.

Two bistatic TDX pairs were used for interferometric processing. The image pairs were acquired on August 14, 2012, and June 5, 2014, from ascending tracks looking right. Imaging was carried out using StripMap mode with an incidence angle of 48°, and, the reported resolution of the original data was 2.4 m in ground range and 3.3 m in azimuth. The height of ambiguity (height corresponding to one interferogram fringe) was around 45 m for both image pairs. The interferometric baseline was 192 m for the 2012 image pair and 190 m for

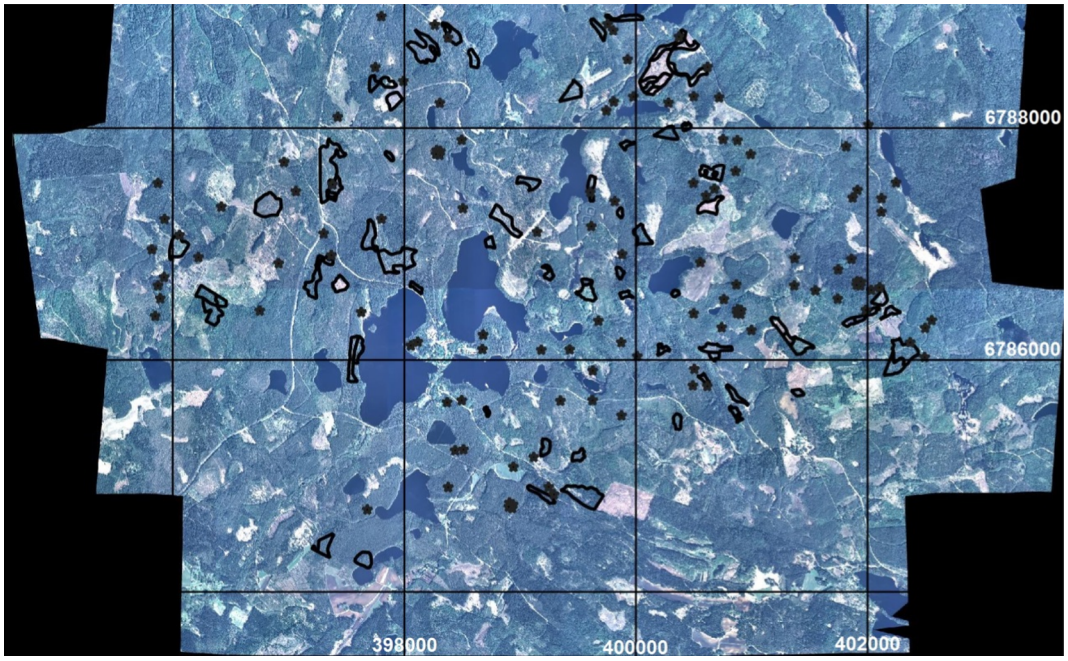

Fig. 1. The aerial image 2014 (©NLS 2014), 364 field plots (a black star on the map presents four 16 × 16 m plots) for reference AGB estimation from ALS, and forest stands (black polygons, see 2.3) for change detection analyses.

the 2014 image pair. On August 14, 2012, the temperature was 23 °C and relative humidity was 49%. On June 5, 2014, the temperature was 16 °C and relative humidity was 84%. Some light rain showers occurred in the nearby areas, but precipitation data was not available for the study site, and thus, local rain showers cannot be excluded.

There are temporal differences between the ALS (May 2012) and TDX (August 2012) datasets. However, the number of harvests during the summer months is typically limited, and also, according to a visual inspection, logging occurred only a few times between the data acquisitions.

Aerial orthoimages acquired on May 7, 2012 (open data set), and May 22, 2014, by NLS, and were used for visual analysis of changed areas. Forest stand borders were available in vector format from an existing forest management plan created by Häme University of Applied Sciences (Fig. 1).

2.2. Calculating biomass-related features from bi-temporal ALS data and classification of stands into four change classes

Features describing canopy height and canopy cover density were derived from the 2012 and 2014 ALS datasets. Features were calculated for grid cells of 16 × 16 m. To describe tree height, the 90th percentile of canopy height distribution (H90) was calculated from the normalized points above the 2 m threshold. The Pearson correlation coefficient (R) between tree height and H90 was estimated using the field plots to be 0.92. Vegetation density was described by the penetration rate (PR) as the ratio of ground returns (points below or equal to 2 m) to the total number of returns. If points above 2 m were not available, the PR was set to 100%. Change features were calculated as differences between features in 2012 and 2014.

$$\Delta height = H90_{2014} - H90_{2012} \quad \text{(positive change means tree growth)}$$

$$\Delta cover = PR_{2012} - PR_{2014} \quad \text{(positive change means more dense vegetation)}$$

The mean for each forest stand was also calculated. Changes in ALS features for forest stands are presented in Fig. 2a and for grid cells in Fig. 2b. The stands were classified into four different change classes (A, B, C, D) based on the mean values of bi-temporal ALS features (Fig. 2a).

2.3. Selecting samples from each change class and visual interpretation

For further analysis, 19 stands were systematically selected from each of the classes A, B, C and D. The stands were drawn randomly from the class and accepted if they passed a visual inspection. In the visual interpretation based on the 2012 and 2014 aerial images, it was verified that the selected stand contains forest or a forest change area. Stands representing clear cut were selected from class A (density decrease and height loss). 7 of the 19 stands were only partially clear cut. Thinnings were selected from class B (density decrease and height increase) based on Δ*cover* and verified from aerial images. However, the change could not be absolutely verified as thinning in all cases (6 of the 19 stands); some minor changes in forest were visible that could have been also blowdown or snow-damaged trees or due to a different phenological stage.

From classes C and D, 19 forest stands were randomly drawn from the class and verified from aerial images as containing homogenous forest. Stands selected from D (height and density increase) present natural growth in this study. Class C contains other changes. Based on a visual interpretation, class C contains sparse and slightly non-homogenous forest stands. Seed tree removals and thinning of the dominant tree layer (typical, if continuous cover forestry is applied) are possible reasons for these changes; however, possible errors due to sparse vegetation cannot be neglected.

The selected stands vary in size (0.1 ha to 4 ha). For the selected stands, the mean AGB in 2012 was 112.0 Mg/ha, the minimum AGB was 26.9 Mg/ha, and maximum the AGB was 209.8 Mg/ha. In this study, the stands are used to extract a total of 2235 grid cells (16 × 16 m) inside the stands for further analysis. For the corresponding grid cells, the mean AGB in 2012 was 101.4 Mg/ha, the minimum AGB was 20.2 Mg/ha, and the maximum was 223.0 Mg/ha. It should be noted that a stand may contain grid cells that would present several classes.

2.4. Predicting above-ground biomass for the grid cell within sample stands using ALS and field observations

Reference AGB maps were produced for 2012 and 2014 using ALS data and the 364 field plots of 16 × 16 m. A digital terrain model (DTM) calculated from ALS was used for ground height. Using the 364 field plots for training, AGB was estimated with the random forest

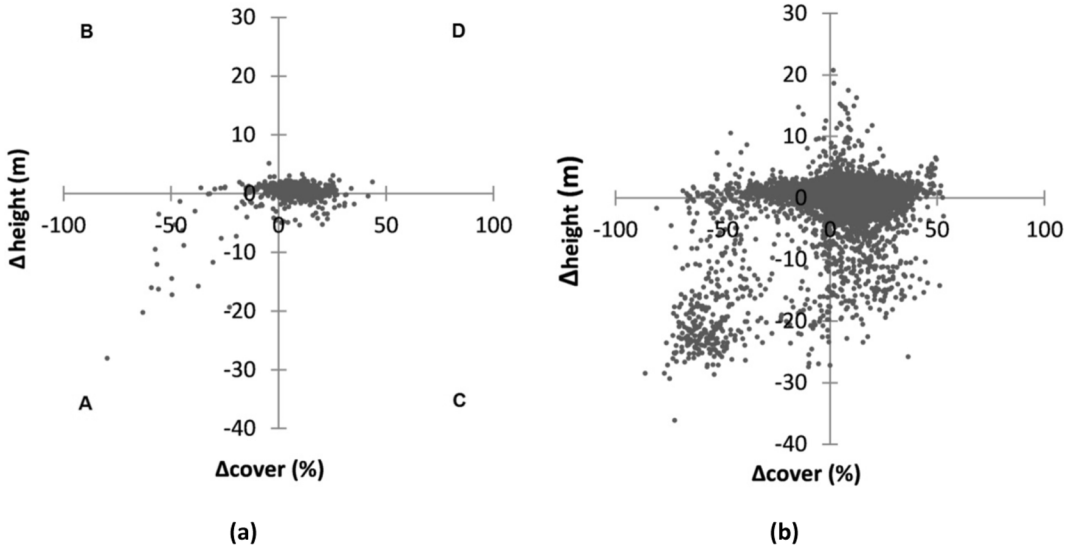

Fig. 2. (a) The ALS change features Δ*cover* and Δ*height* at forest stand level; **(b)** for grid cells (right). On the left is the classification into four different change classes: A, B, C and D.

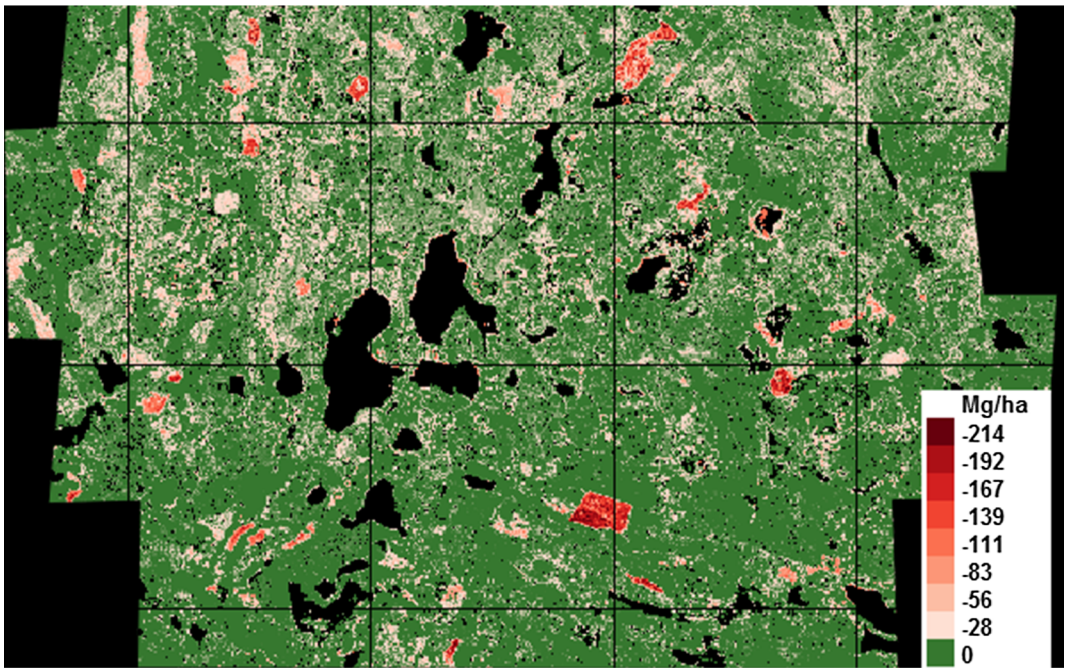

Fig. 3. The AGB change map (Mg/ha) derived from field data and ALS datasets using random forest method.

technique (Yu et al., 2015). The root-mean-square error (RMSE) of the AGB estimation was approximately 28 Mg/ha (21%) (Yu et al., 2015). AGB maps of the study area were predicted for 2012 and 2014 with a 16 × 16 m pixel size, and a change map was produced by subtracting the 2014 AGB map from the 2012 AGB map (Fig. 3)

The average AGB change was −92.4 Mg/ha for the stands included in the change class clear cut (A), −29.1 Mg/ha for class thinning (B), −11.7 Mg/ha for class other changes (C), and 3.6 Mg/ha for class growth (D).

2.5. Deriving digital surface models from interferometric SAR data for 2012 and 2014 and calculating features

Tandem-X DSMs were produced using the interferometric SAR (InSAR) processing chain in ENVI/SARscape software with a pixel size of 4 × 4 m, described in more detail in (Karila et al., 2015). InSAR DSMs contain relative height values, and they need to be matched using common reference points or areas in open areas. In this study, InSAR heights were matched to ALS DTM using nine reference areas (mostly fields or meadows) to get absolute heights. Low coherence areas (coherence less than 0.25) were set as no data during the InSAR processing.

To calculate the features from bi-temporal InSAR DSMs, the 16 × 16 m grid was used. For each grid cell the minimum, maximum, mean and standard deviation of the InSAR heights were calculated. A height difference map was derived from InSAR DSMs (2014–2012) and resampled to the 16 × 16 m grid size.

2.6. Investigating forest biomass, height and density changes by change classes

ALS and InSAR features were compared for the change classes: clear cut (A), thinning (B), other changes (C), and growth (D). For each grid

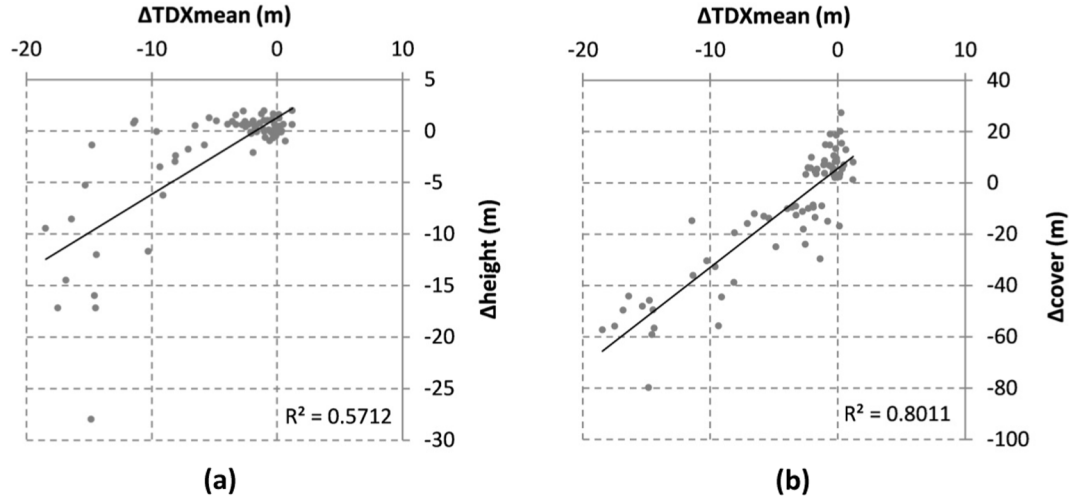

Fig. 4. Stand-level comparison of change in Tandem-X mean height (Δ*TDXmean*) and **(a)** ALS-derived change in 90th height percentile (Δ*height*), and **(b)** change in penetration rate (Δ*cover*), for all classes.

cell inside the 19 selected stands, the difference of InSAR features in 2012 and 2014 was calculated to derive Δ*TDXmin*, Δ*TDXmean*, Δ*TDXmax*, and Δ*TDXstd*. The correlation between Δ*height* and Δ*cover* from ALS and InSAR change features was calculated for the grid cells.

2.7. Predicting biomass change using InSAR change features

In previous studies, both linear (e.g. Solberg et al., 2014; Næsset et al., 2015) and nonlinear regression models (e.g. Solberg et al., 2010, 2013; Soja et al., 2015) have been used for biomass estimation from InSAR height. The advantage of linear models is that positive and negative values can be used. Therefore, the model describes both the biomass growth and loss. Direct methods estimate AGB change directly from height change (ΔH), and, indirect methods estimate first AGB for both dates and the difference is calculated to obtain the biomass change.

In this study, AGB prediction models based on TDX estimates of InSAR height were developed by using the 16 × 16 m grid cells inside the 76 selected forest stands (See 2.3). Linear models (1) with and without intercept were developed and the accuracy was calculated using the root-mean-square error (RMSE). Nonlinear models (2) were developed for a subset of data including the positive values of biomass loss and height loss. Indirect linear models (3) were also tried. The models used were:

$$\Delta AGB = a \cdot \Delta H\,(+b) \quad (1)$$

$$\Delta AGB = a \cdot \Delta H^{b}(+c) \quad (2)$$

$$\Delta AGB = a \cdot H_{2012} + b \cdot H_{2014}(+c) \quad (3)$$

where ΔH is the TDX height change, H_{2012} and H_{2014} are the TDX mean heights in 2012 and 2014 respectively, and a, b and c are the unknown parameters.

Finally, the AGB prediction model was validated at grid cell level by using a modified k-fold cross-validation in which one stand out of the 76 stands was left out and the model was defined with the grid cells of the other 75 stands. The difference between the observed and predicted value was determined for each grid cell inside the left-out stand. This was repeated for all 76 stands. The $RMSE_{gc\_CV}$ was calculated from the differences between prediction and observation for each grid cell of all estimation rounds. Stand-level AGB change values were obtained by aggregating all the predicted grid values within a stand. The root-mean-square error $RMSE_{s\_CV}$ was calculated from the stand-level differences between observed and predicted values of all estimation rounds.

$$RMSE_{CV} = \sqrt{\frac{\sum_{i=1}^{n} (\Delta AGB_{obs} - \Delta AGB_{pred})^2}{n}} \quad (4)$$

where n is the number of grid cells ($RMSE_{gc\_CV}$) or stands ($RMSE_{s\_CV}$).

Finally, an AGB change map was predicted for the whole study area, and the estimates were compared to the ALS-based AGB change map and aerial orthoimages.

3. Results

3.1. Comparison of ALS and InSAR changes features

First, InSAR and ALS change features were compared at forest stand level (Fig. 4) using all of the selected 76 stands. At stand level, the coefficient of determination R^2 for Δ*height* and Δ*TDXmean* was 0.57 (Pearson correlation coefficient $R = 0.76$). For Δ*cover* and Δ*TDXmean,* the coefficient of determination was higher: 0.80 ($R = 0.89$).

At the grid cell level R^2 for Δ*height* and Δ*TDXmean* was 0.44 ($R = 0.66$) and for Δ*cover* and Δ*TDXmean* R^2 was 0.69 ($R = 0.83$). For grid cells inside forest stands of classes A, B, C and D, the results are presented in Table 1. Δ*height* and Δ*cover* both correlated with changes in InSAR height (Δ*TDXmean*, Δ*TDXmin* and Δ*TDXmax*) for the clear cut (A) and thinning (B) classes. However, the correlation was weaker than at stand level. The correlation of InSAR height change was stronger for changes in forest density than for changes in forest height. The correlation was similar for Δ*TDXmean*, Δ*TDXmin* and Δ*TDXmax*. Δ*TDXstd* did not correlate strongly with the ALS change features. In interferometric processing, several pixels are averaged and continuity of the interferometric phase is favored (filtering and phase unwrapping steps). Therefore, there was not much variation in height, and minimum and maximum heights were close to the mean height.

3.2. Predicting biomass changes based on InSAR height

Using the grid cells inside the selected 76 forest stands, the AGB from ALS and InSAR height and their differences were used to derive linear models to predict forest AGB change. For AGB estimation linear model with intercept was selected. Direct and indirect methods were used for the biomass change estimation. Grid cell (gc) level and stand (s) level linear models for AGB in 2012, AGB in 2014 and models for AGB change are presented in Table 2. The original data is presented at stand level in Fig. 5.

Nonlinear regression models were fitted to a subset of the grid cell data including grid cells with observed AGB loss and decrease in

Table 1
The coefficient of determination (R^2) between interferometric SAR (InSAR) change features and airborne laser scanning (ALS) change features for the grid cells of four different change classes. InSAR mean height change (Δ*TDXmean*), change in standard deviation of height (Δ*TDXstd*), change in minimum height (Δ*TDXmin*) and change in maximum height (Δ*TDXmax*) were compared to ALS-derived change in 90th height percentile (Δ*height*) and change in penetration rate (Δ*cover*).

	Clear cut (A)		Thinning (B)		Other changes (C)		Growth (D)	
	Δ*height*	Δ*cover*	Δ*height*	Δ*cover*	Δ*height*	Δ*cover*	Δ*height*	Δ*cover*
Δ*TDXmean*	0.190*	0.444*	0.020*	0.155*	0.003	0.009*	0.001	0.030*
Δ*TDXstd*	0.018*	0.018*	0.001	0.004	0.000	0.001	0.002	0.000
Δ*TDXmin*	0.161*	0.403*	0.016*	0.173*	0.003	0.005	0.003	0.023*
Δ*TDXmax*	0.180*	0.400*	0.017*	0.118*	0.001	0.010*	0.000	0.031*

* The correlation is statistically significant: p-value < 0.05.

Table 2
Linear models for AGB and AGB change estimation from Tandem-X height (H) at stand (s) and grid cell (gc) level.

Model	Level	Equation	RMSE (Mg/ha)	Equation number
AGB 2012	Grid cell	$AGB_{2012\_gc} = 7.04 \cdot H_{2012} + 37.40$	29.6	(5)
AGB 2014	Grid cell	$AGB_{2014\_gc} = 6.92 \cdot H_{2014} + 35.95$	29.7	(6)
AGB 2012	Stand	$AGB_{2012\_s} = 7.04 \cdot H_{2012} + 40.55$	21.8	(7)
AGB 2014	Stand	$AGB_{2014\_s} = 6.24 \cdot H_{2014} + 43.44$	22.6	(8)
ΔAGB indirect	Grid cell	$\Delta AGB_{gc} = 5.50 \cdot H_{2012} - 6.35 \cdot H_{2014} + 12.43$	26.3	(9)
ΔAGB indirect	Stand	$\Delta AGB_{s} = 6.09 \cdot H_{2012} - 6.98 \cdot H_{2014} + 11.16$	20.0	(10)
ΔAGB direct	Grid cell	$\Delta AGB_{gc} = 6.39 \cdot \Delta H$	27.1	(11)
ΔAGB direct	Grid cell	$\Delta AGB_{gc} = 5.85 \cdot \Delta H + 6.51$	26.6	(12)
ΔAGB direct	Stand	$\Delta AGB_{s} = 6.90 \cdot \Delta H$	20.3	(13)

Tandem-X height (1428 grid cells). For comparison, linear models were fitted using the same subset of data. The nonlinear models derived were:

$$\Delta AGB_{gc} = 13.63 \cdot \Delta H^{0.72} \text{ (RMSE 26.4 Mg/ha)} \quad (14)$$

$$\Delta AGB_{gc} = 2.92 \cdot \Delta H^{1.22} + 17.20 \text{ (RMSE 25.5 Mg/ha)} \quad (15)$$

Using the same subset linear model had an RMSE of 25.6 Mg/ha (slope 5.52 and intercept 13.38). Therefore, there is no significant advantage in using the nonlinear model.

For direct AGB change estimation at stand level the intercept of the linear was not significant. At grid cell level accuracy increase was minor when intercept was included. Also, the indirect models resulted in only a minor increase in accuracy in comparison to direct models.

Finally, the performance of direct linear no-intercept models for AGB estimation was evaluated using the modified k-fold cross validation (see Section 2.7). The observed and predicted AGB changes were compared using the ALS-based AGB change as reference (Fig. 6). $RMSE_{gc\_CV}$ was 27.4 Mg/ha (27.0% of the original AGB in 2012) and $RMSE_{s\_CV}$ 20.7 Mg/ha (18.5%).

Finally, to derive an AGB change map of the study area from TDX height change, linear model (11) was used. For visual analysis, the AGB change was predicted for the whole study area using the 16 × 16 m grid cells (Fig. 7). Close-ups of the AGB change predictions and the corresponding aerial orthoimages are presented in Fig. 8.

4. Discussion

In our study, vegetation height and density changes resulted in consistent changes in InSAR height features. Grid cell correlation analysis showed that changes are detectable at sub-stand level. TDX height change was estimated to correlate more with density change than with height change. This is related to the phase center height being

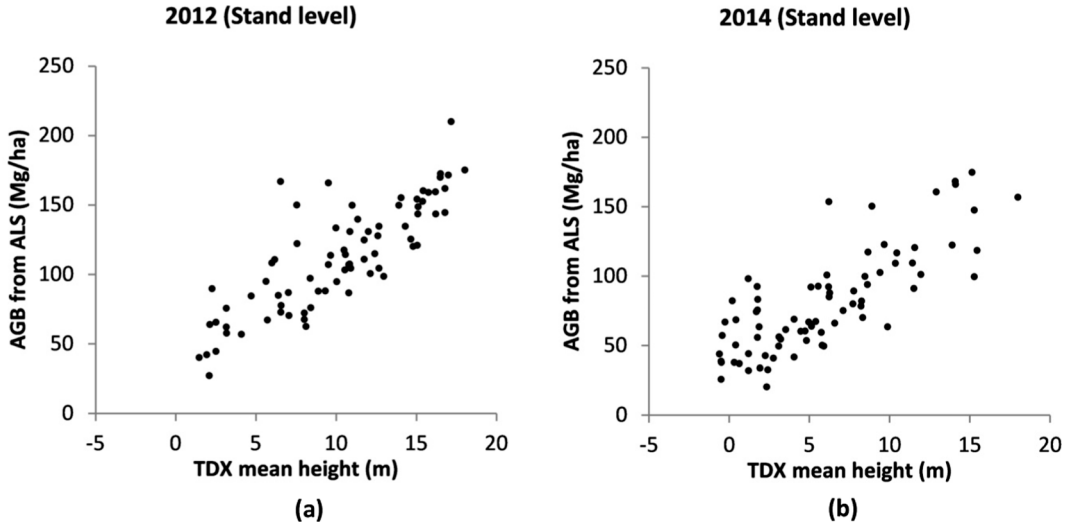

Fig. 5. TDX mean height of stands and AGB in 2012 **(a)**, and 2014 **(b)**.

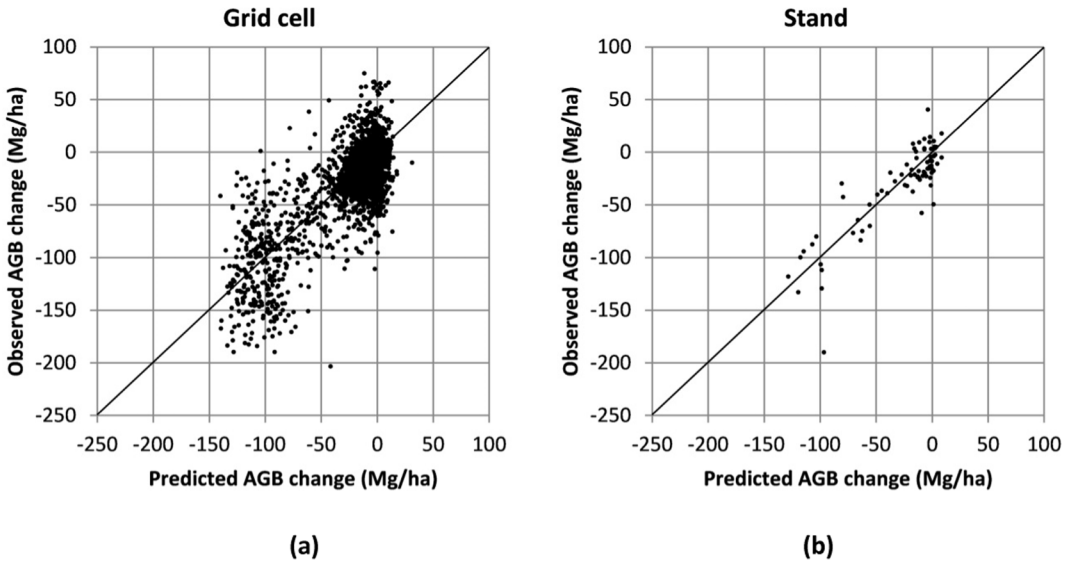

Fig. 6. (**a**) The observed AGB change (estimated from bi-temporal ALS and field data) vs. predicted AGB change from TanDEM-X interferometric height change resulting from the modified k-fold cross validation at grid cell level. (**b**) The observed AGB change (estimated from bi-temporal ALS and field data) vs. predicted AGB change from TanDEM-X interferometric height change resulting from the leave-one-out validation at stand level. 1:1 line is presented in the figure.

dependent on the penetration into forest canopy which is affected by the density (Hagberg et al., 1995; Treuhaft and Siqueira, 2004). Also, InSAR produces a smooth surface DSM that is not as sensitive to abrupt changes (or detailed) as ALS DSM. Some changes e.g. due to growth occur throughout the area but some changes are very local e.g. resulting from single cut down trees. Often a change in the forest results in both height and density changes. In the data used in this study forest height (H90) change and density change had a moderate correlation ($R = 0.59$), which is caused by the type of changes e.g. including clear cuts in the data. In general, forest type affects the correlation between forest height and density, and, in the study area the correlation is weak ($R = -0.23$). For other type of forest and other type of changes the correlation between TDX height change and forest height or density changes may be different.

Forest height loss due to clear cuts was detected, and the correlation with InSAR height change was strong. Thinnings had a moderate correlation to TDX height changes. The results support findings by Persson et al. (2015) that clear cuts are easily detected and thinnings are detectable to some extent. The data acquisition interval was only two years, and the expected forest height increase due to growth was rather small. The InSAR datasets used in this study were not able to detect growth in the two-year time period. For the change class growth (D), the average change in height detected from ALS was only 60 cm. Differences in SAR signal penetration into canopy due to environmental conditions, and, any inaccuracies in height level matching of the InSAR DSMs, for example due to vegetation height in open areas, may affect the detection of growth. However, over a considerably longer time span, forest growth causing a large increase in density or height should

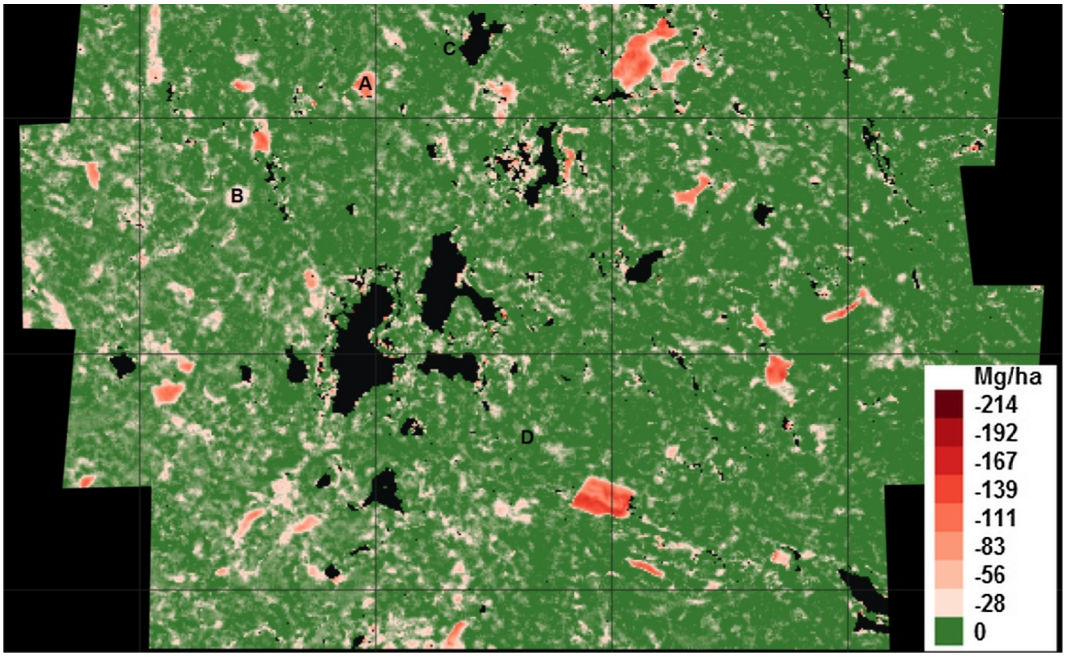

Fig. 7. AGB change map (Mg/ha) in 16 × 16 m cell size predicted from TDX height changes using a linear model (11). Black areas present no data areas. The locations for the subsets in Fig. 8 are marked with letters A–D.

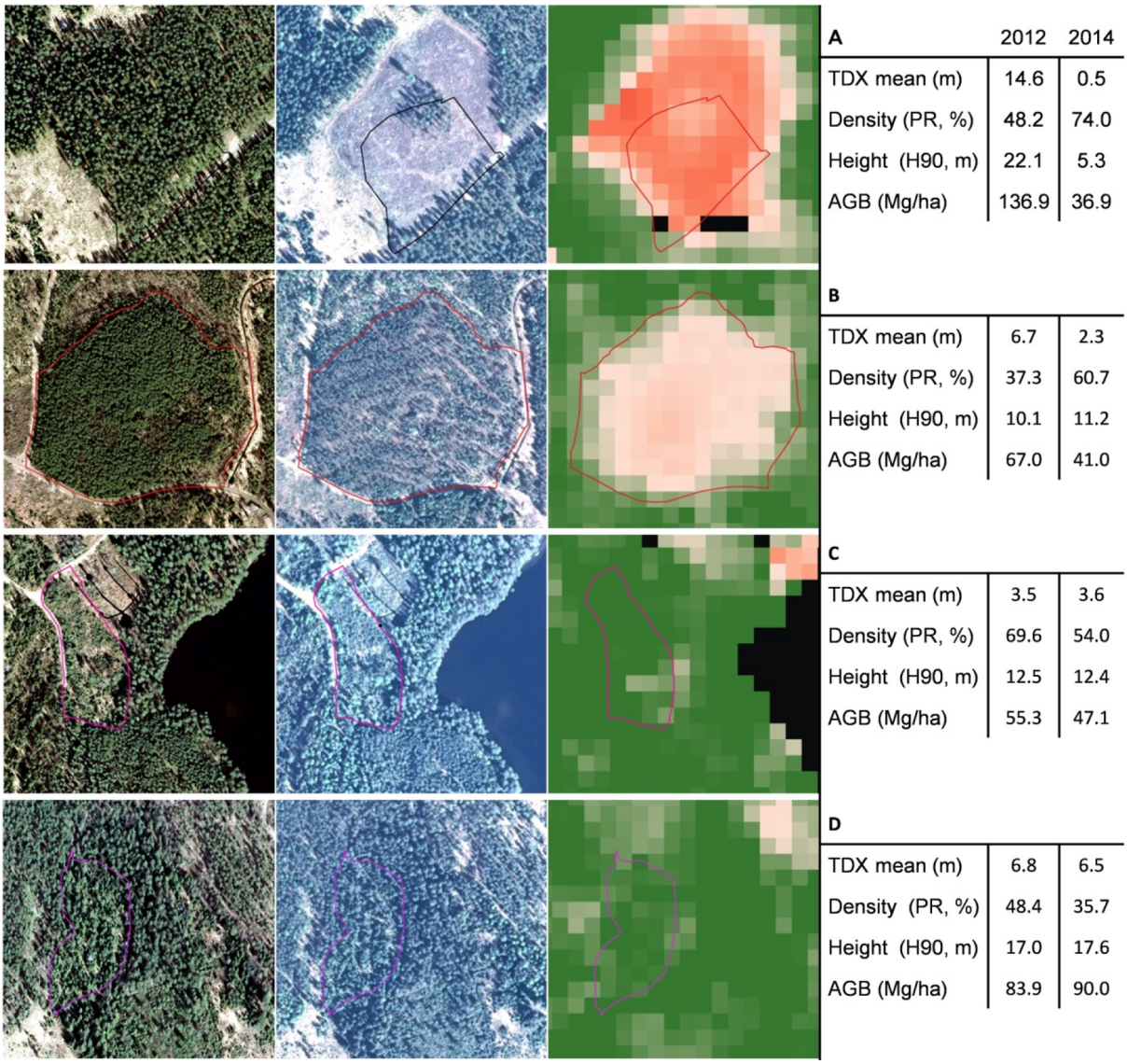

Fig. 8. Close-ups of AGB change predicted from TanDEM-X interferometric height change and corresponding aerial image subsets. These four subsets present different change classes (from top down): clear cut (A), thinning (B), other changes (C), and growth (D). Polygons present the stand borders. Aerial orthoimage 2012 (left, ©NLS 2012), aerial orthoimage 2014 (middle, ©NLS 2014), AGB change predicted from TDX (right) for grid cells of 16 × 16 m. The AGB change color bar can be found in Fig. 7.

be detectable from a single InSAR DSM difference, since large decreases in forest density and height were reliably detected. In Askne et al. (2018), growth could be detected over a 3.2-year period using a large set of TDX acquisitions.

We detected AGB changes of different orders of magnitude using TDX height changes and a simple model. Visual analysis using aerial orthoimages as well as the numerical validation using the selected stands showed correlation between the AGB changes predicted, AGB changes estimated from ALS data, and visible forest changes. However, it should be noted that the model is only applicable to forests similar to the study area, and different models and parameters are needed for different types of forest. The AGB models derived (5)-(8) are similar to models derived by Solberg et al. (2010) for pine dominated forest using X-band SRTM data (AGB = 43 + 6.8H). In other studies considering boreal forest, the slope has been found higher; In Soja et al. (2015) for two sites in Sweden using several Tandem-X acquisitions simple no-intercept linear models had slopes of 8.3–9.6 and 11.3–12.2; In Næsset et al. (2015) for pine dominated forest using TDX slope was 11.1 (intercept 18.4); and in Solberg et al. (2014) for spruce dominated forest using TDX slope was 14.9. So, there is variation in model parameters for boreal forest and for other forest types (tropical, temperate) even more variation is expected.

Nonlinear relations between phase height and AGB have been proposed in previous studies (Soja et al., 2015; Askne et al., 2018; Knapp et al., 2018). However, the dataset used in this study could not verify this. It may be due to the limited size of the dataset and limited occurrence of changes of different magnitudes or the amount of change vs. no change. However, also in previous studies nonlinear relationships could not have been verified (Solberg et al., 2010, 2013). Often, curvilinear relationships have been proposed for biomass using tree height as a predictor; however, interferometric height is more related to canopy height and gaps in canopy than the tree height (Solberg et al., 2013). In addition, different forest types and baseline geometries might affect the modeling. In this study the Tandem-X pairs used have very similar imaging geometry. For TDX pairs acquired using different geometries the model may be more complex.

The variance in the grid-based comparison of TDX and ALS changes was likely due the side-looking imaging geometry of SAR. As a result, at

the grid cell level, the SAR measurement may have originated from a different object than the ALS measurement (Næsset et al., 2015). In addition, the TDX DSM had a smooth surface and the variations in height were smaller than for ALS. Area-based ALS methods have been proved to provide accurate predictions for forest inventory attributes that are highly correlated with canopy height and density, such as AGB. In boreal forest conditions, ALS-based predictions for stem volume or AGB typically have an RMSE of approximately 20% at the plot level (sample plot size ranging from 100 to 300 m^2) (e.g. Vastaranta et al., 2013, Yu et al., 2010) but it decreases closer to, or even below, 10% at the stand level (e.g. Maltamo et al., 2006). Therefore, the use of large sample plots (> 500 m^2) or stands for validation has been found preferable when references are obtained using ALS (Næsset et al., 2015; Yu et al., 2015). The 16 × 16 m grid cells used in this study may not be of optimal size for comparisons with ALS data.

Our results are in line with other studies using InSAR DSMs for direct AGB change estimation. In Næsset et al. (2015), the AGB change was estimated using a linear model and the height difference between interferometric data from TDX and SRTM. For mature pine-dominated forest in Norway, the RMSE was 24.8 Mg/ha (400 m^2 plots) and 30.2 Mg/ha (200 m^2 plots). In Solberg et al. (2014), which also used TDX and SRTM datasets, the RMSE was 59 Mg/ha.

The limitations of the InSAR DSM-based forest change detection technique are related to the quality of input data. The availability of two suitable TDX pairs is essential to the technique. Different imaging geometries, different time of the year or weather conditions of the pairs might affect the interferometric height (Kugler et al., 2014) and the accuracy of the AGB change estimate. In addition, low coherence areas are not used in generating digital surface model because the quality of the phase information is not adequate. Therefore, there are gaps in the final AGB change map from a single TDX image pair. The coherence is strongly influenced by incidence angle, and combining DSMs produced using image pairs with different imaging geometries would help in filling the gaps. However, in our study area only approximately 10% of pixels (excluding water areas) were not included in the result, and good coverage of the area was obtained.

5. Conclusions

This study shows that abrupt AGB change in boreal forests can be estimated using interferometric DSM height differences from the TDX mission and a simple model. Based on our results, InSAR height changes correlate more with forest density changes than forest height changes. However, in comparison to ALS measurements, for short acquisition intervals there is remarkable variance in the TDX height differences for individual grid cells. Considering the information needs in planning sustainable forest management and carbon monitoring, sub-stand-level drastic negative changes in AGB are detectable with InSAR. Forest structural changes over wide areas can be mapped if suitable InSAR pairs are available. It was also shown that the detected changes can be linked to the AGB change.

Acknowledgments

The field data from Evo was collected by research groups lead by Juha Hyyppä, Markus Holopainen and Masato Katoh. The authors are grateful to Lic. Sc. Risto Viitala and Häme University of Applied sciences for all the help with practical arrangements at Evo, and to Kimmo Nurminen for processing the aerial orthoimage mosaic from 2014. The Tandem-X data was provided by the DLR through the DLR TDX scientific project ID XTI_VEGE0360. This research was funded by the European Community's Seventh Framework Programme (FP7/2007–2013) [grant number 606971], and the Academy of Finland [grant numbers 277734, 307362].

References

Askne, J.I., Dammert, P.B., Ulander, L.M., Smith, G., 1997. C-band repeat-pass interferometric SAR observations of the forest. IEEE Trans. Geosci. Remote Sens. 35, 25–35.
Askne, J.I., Fransson, J.E., Santoro, M., Soja, M.J., Ulander, L.M., 2013. Model-based biomass estimation of a hemi-boreal forest from multitemporal TanDEM-X acquisitions. Remote Sens. 5, 5574–5597.
Askne, J.I., Santoro, M., 2015. On the estimation of boreal Forest biomass from TanDEMX data without training samples. IEEE Geosci. Remote Sens. Lett. 12, 771–775.
Askne, J.I., Soja, M.J., Ulander, L.M., 2017. Biomass estimation in a boreal forest from TanDEM-X data, lidar DTM, and the interferometric water cloud model. Remote Sens. Environ. 196, 265–278.
Askne, J.I., Persson, H.J., Ulander, L.M., 2018. Biomass growth from multi-temporal TanDEM-X interferometric synthetic aperture radar observations of a boreal forest site. Remote Sens. 10, 603.
Bouvier, M., Durrieu, S., Fournier, R.A., Renaud, J., 2015. Generalizing predictive models of forest inventory attributes using an area-based approach with airborne LiDAR data. Remote Sens. Environ. 156, 322–334.
Bradshaw, C.J.A., Warkentin, I.G., 2015. Global estimates of boreal forest carbon stocks and flux. Global Planet. Change 128, 24–30.
Bamler, R., Hartl, P., 1998. Synthetic aperture radar interferometry. Inverse Prob. 14, R1–R54.
Boisvenue, C., Smiley, B.P., White, J.C., Kurz, W.A., Wulder, M.A., 2016. Improving carbon monitoring and reporting in forests using spatially-explicit information. Carb. Balance Manag. 11, 23.
Bonan, G.B., 2008. Forests and climate change: forcings, feedbacks, and the climate benefits of forests. Science 320, 1444–1449.
Cao, L., Coops, N.C., Innes, J.L., Sheppard, S.R.J., Fu, L., Ruan, H., She, G., 2016. Estimation of forest biomass dynamics in subtropical forests using multi-temporal airborne LiDAR data. Remote Sens. Environ. 178, 158–171.
Drusch, M., Del Bello, U., Carlier, S., Colin, O., Fernandez, V., Gascon, F., Hoersch, B., Isola, C., Laberinti, P., Martimort, P., Meygret, A., Spoto, F., Sy, O., Marchese, F., Bargellini, P., 2012. Sentinel-2: ESA's optical high-resolution mission for GMES operational services. Remote Sens. Environ. 120, 25–36.
European Energy Exchange (EEX): EU Emission Allowances. Available online: https://www.eex.com/en/market-data/environmental-markets/spot-market/european-emission-allowances#!/2017/03/13 (Accessed on 13 March 2018).
Eurostat: Forestry and climate change. Available online: http://ec.europa.eu/eurostat/statistics-explained/index.php/Forestry_and_climate_change (Accessed on 13 March 2018).
Hagberg, J.O., Ulander, L.M., Askne, J.I., 1995. Repeat-pass interferometry over forested terrain. IEEE Trans. Geosci. Remote Sens. 33, 331–340.
Hansen, M.C., Potapov, P.V., Moore, R., Hancher, M., Turubanova, S.A., Tyukavina, A., Thau, D., Stehman, S.V., Goetz, S.J., Loveland, T.R., Kommareddy, A., Egorov, A., Chini, L., Justice, C.O., Townshend, J.R.G., 2013. High-resolution global maps of 21st-century forest cover change. Science 342 (6160), 850–853.
Hansen, E.H., Gobakken, T., Solberg, S., Kangas, A., Ene, L., Mauya, E., Næsset, E., 2015. Relative efficiency of ALS and InSAR for biomass estimation in a tanzanian rainforest. Remote Sens. 7, 9865–9885.
Hermosilla, T., Wulder, M.A., White, J.C., Coops, N.C., Hobart, G.W., 2015. Regional detection, characterization, and attribution of annual forest change from 1984 to 2012 using Landsat-derived time-series metrics. Remote Sens. Environ. 170, 121–132.
Houghton, R., 2005. Aboveground forest biomass and the global carbon balance. Glob. Chang. Biol. 11, 945–958.
Hyyppä, J., Hyyppä, H., Leckie, D., Gougeon, F., Yu, X., Maltamo, M., 2008. Review of methods of small-footprint airborne laser scanning for extracting forest inventory data in boreal forests. Int. J. Remote Sens. 29, 1339–1366.
Kaasalainen, S., Krooks, A., Liski, J., Raumonen, P., Kaartinen, H., Kaasalainen, M., Puttonen, E., Anttila, K., Mäkipää, R., 2014. Change detection of tree biomass with terrestrial laser scanning and quantitative structure modelling. Remote Sens. 6, 3906–3922.
Kankare, V., Vastaranta, M., Holopainen, M., Räty, M., Yu, X., Hyyppä, J., Hyyppä, H., Alho, P., Viitala, R., 2013. Retrieval of forest aboveground biomass and stem volume with airborne scanning LiDAR. Remote Sens. 5, 2257–2274.
Karila, K., Vastaranta, M., Karjalainen, M., Kaasalainen, S., 2015. Tandem-X interferometry in the prediction of forest inventory attributes in managed boreal forests. Remote Sens. Environ. 159, 259–268.
Knapp, N., Huth, A., Kugler, F., Papathanassiou, K., Condit, R., Hubbell, S.P., Fischer, R., 2018. Model-assisted estimation of tropical forest biomass change: a comparison of approaches. Remote Sens. 10 (5), 717.
Koch, B., 2010. Status and future of laser scanning, synthetic aperture radar and hyperspectral remote sensing data for forest biomass assessment. ISPRS J. Photogramm. Remote Sens. 65 (6), 581–590.
Kugler, F., Schulze, D., Hajnsek, I., Pretzsch, H., Papathanassiou, K., 2014. TanDEM-X Pol-InSAR performance or forest height estimation. IEEE Tran. Geosci. Remote Sens. 52 (10), 6404–6422.
Krieger, G., Moreira, A., Fiedler, H., Hajnsek, I., Werner, M., Younis, M., Zink, M., 2007. TanDEM-X: a satellite formation for high-resolution SAR interferometry. IEEE Trans. Geosci. Remote Sens. 45, 3317–3341.
Lunetta, R.S., Johnson, D.M., Lyon, J.G., Crotwell, J., 2004. Impacts of imagery temporal frequency on land-cover change detection monitoring. Remote Sens. Environ. 89 (4), 444–454.
Maltamo, M., Malinen, J., Packalén, P., Suvanto, A., Kangas, J., 2006. Non-parametric

estimation of stem volume using laser scanning, aerial photography and stand register data. Can. J. For. Res. 36, 426–436.
Mette, T., Hajnsek, I., Papathanassiou, K., 2003. Height-biomass allometry in temperate forests performance accuracy of height-biomass allometry. In: Proceedings of 2003 IEEE International Geoscience and Remote Sensing Symposium, Toulouse, France, 21-25 July 2003, pp. 1942–1944.
Næsset, E., 2007. Airborne laser scanning as a method in operational forest inventory: status of accuracy assessments accomplished in Scandinavia. Scand. J. For. Res. 22, 433–442.
Næsset, E., Bollandsås, O.M., Gobakken, T., Gregoire, T.G., Ståhl, G., 2013. Model-assisted estimation of change in forest biomass over an 11year period in a sample survey supported by airborne LiDAR: A case study with post-stratification to provide "activity data". Remote Sens. Environ. 128, 299–314.
Næsset, E., Bollandsås, O.M., Gobakken, T., Solberg, S., McRoberts, R.E., 2015. The effects of field plot size on model-assisted estimation of aboveground biomass change using multitemporal interferometric SAR and airborne laser scanning data. Remote Sens. Environ. 168, 252–264.
Økseter, R., Bollandsås, O.M., Gobakken, T., Næsset, E., 2015. Modeling and predicting aboveground biomass change in young forest using multi-temporal airborne laser scanner data. Scand. J. For. Res. 30 (5), 1651–1891.
Persson, H., Wallerman, J., Olsson, H., Fransson, J.E., 2013. Estimating forest biomass and height using optical stereo satellite data and a DTM from laser scanning data. Can. J. Remote Sens. 39 (3), 251–262.
Persson, H.J., Soja, M.J., Ulander, L.M., Fransson, J.E., 2015. Detection of thinning and clear-cuts using TanDEM-X data. In: Proceedings of 2015 IEEE International Geoscience and Remote Sensing Symposium, Milan, Italy, 26-31 July 2015, pp. 2907–2910.
Persson, H.J., 2016. Estimation of boreal forest attributes from very high resolution pléiades data. Remote Sens. 8, 736.
Persson, H.J., Fransson, J.E., 2017. Comparison between TanDEM-X- and ALS-based estimation of aboveground biomass and tree height in boreal forests. Scand. J. For. Res. 32 (4), 306–319.
Persson, H.J., Olsson, H., Soja, M.J., Ulander, L.M., Fransson, J.E., 2017. Experiences from large-scale forest mapping of sweden using TanDEM-X Data. Remote Sens. 9, 1253.
Praks, J., Antropov, O., Hallikainen, M.T., 2012. LIDAR-aided SAR interferometry studies in boreal forest: Scattering phase center and extinction coefficient at X- and L-band. IEEE Trans. Geosci. Remote Sens. 50, 3831–3843.
Repola, J., 2008. Biomass equations for birch in Finland. Silva Fennica. 42, 605–624.
Repola, J., 2009. Biomass equations for Scots pine and Norway spruce in Finland. Silva Fennica. 43, 625–647.
Sarabandi, K., Lin, Y.C., 2000. Simulation of interferometric SAR response for characterizing the scattering phase center statistics of forest canopies. IEEE Trans. Geosci. Remote Sens. 39, 115–125.
Solberg, S., Astrup, R., Gobakken, T., Næsset, E., Weydahl, D.J., 2010. Estimating spruce and pine biomass with interferometric X-band SAR. Remote Sens Environ. 114, 2353–2360.
Solberg, S., Astrup, R., Breidenbach, J., Nilsen, B., Weydahl, D., 2013a. Monitoring spruce volume and biomass with InSAR data from TanDEM-X. Remote Sens. Environ. 139, 60–67.
Solberg, S., Astrup, R., Weydahl, D.J., 2013b. Detection of forest clear-cuts with shuttle radar topography mission (SRTM) and tandem-X InSAR data. Remote Sens. 5, 5449–5462.
Solberg, S., Næsset, E., Gobakken, T., Bollandsås, O.-M., 2014. Forest biomass change estimated from height change in interferometric SAR height models. Carb. Balance Manag. 9, 5.
Solberg, S., Hansen, E.H., Gobakken, T., Næssset, E., Zahabu, E., 2017. Biomass and InSAR height relationship in a dense tropical forest. Remote Sens. Environ. 192, 166–175.
Soja, M.J., Persson, H.J., Ulander, L.M., 2015a. Estimation of forest biomass from two-level model inversion of single-pass InSAR data. IEEE Trans. Geosci. Remote Sens. 53, 5083–5099.
Soja, M.J., Persson, H.J., Ulander, L.M., 2015b. Estimation of forest height and canopy density from a single InSAR correlation coefficient. IEEE Geosci. Remote Sens. Lett. 12 (3), 646–650.
St-Onge, B., Vega, C., Fournier, R.A., Hu, Y., 2008. Mapping canopy height using a combination of digital stereo-photogrammetry and lidar. Int. J. Remote Sens. 29 (11), 3343–3364.
Torano, C.A., Kugler, F., Hajnsek, I., Papathanassiou, K.P., 2016. Large-scale biomass classification in boreal forests with TanDEM-X data. IEEE Trans. Geosci. Remote Sens. 54 (10), 5935–5951.
Treuhaft, R.N., Siqueira, P.R., 2004. The calculated performance of forest structure and biomass estimates from interferometric radar. Waves Random Media 14 (2), 345–358.
Treuhaft, R., Lei, Y., Gonçalves, F., Keller, M., Santos, J.R., Neumann, M., Almeida, A., 2017. Tropical-forest structure and biomass dynamics from TanDEM-X radar interferometry. Forests 8, 277.
Tian, J., Schneider, T., Straub, C., Kugler, F., Reinartz, P., 2017. Exploring digital surface models from nine different sensors for forest monitoring and change detection. Remote Sens. 9, 287.
Sheridan, R.D., Popescu, S.C., Gatziolis, D., Morgan, C.L.S., Ku, N.-W., 2015. Modeling forest aboveground biomass and volume using airborne LiDAR metrics and forest inventory and analysis data in the pacific northwest. Remote Sens. 7, 229–255.
Song, C., 2012. Optical remote sensing of forest leaf area index and biomass. Prog. Phys. Geogr. 37 (1), 98–113.
Vastaranta, M., Wulder, M.A., White, J.C., Pekkarinen, A., Tuominen, S., Ginzler, C., Kankare, V., Holopainen, M., Hyyppä, J., Hyyppä, H., 2013. Airborne laser scanning and digital stereo imagery measures of forest structure: comparative results and implications to forest mapping and inventory update. Can. J. Remote Sens. 39 (5), 382–395.
Wagner, W., Luckman, A., Vietmeier, J., Tansey, K., Balzter, H., Schmullius, C., Davidson, M., Gaveau, D., Gluck, M., Le Toan, T., Quegan, S., Shvidenko, A., Wiesmann, A., Yu, J.J., 2003. Large-scale mapping of boreal forest in SIBERIA using ERS tandem coherence and JERS backscatter data. Remote Sens. Environ. 85 (2), 125–144.
Wulder, M.A., Masek, J.G., Cohen, W.B., Loveland, T.R., Woodcock, C.E., 2012. Opening the archive: How free data has enabled the science and monitoring promise of Landsat. Remote Sens. Environ. 122, 2–10.
Yu, X., Hyyppä, J., Kaartinen, H., Maltamo, M., Hyyppä, H., 2008. Obtaining plotwise mean height and volume growth in boreal forests using multi-temporal laser surveys and various change detection techniques. Int. J. Remote Sens. 29 (5), 1367–1386.
Yu, X., Hyyppä, J., Holopainen, M., Vastaranta, M., 2010. Comparison of area-based and individual tree-based methods for predicting plot-level forest attributes. Remote Sens. 2, 1481–1495.
Yu, X., Hyyppä, J., Karjalainen, M., Nurminen, K., Karila, K., Vastaranta, M., Kankare, V., Kaartinen, H., Holopainen, M., Honkavaara, E., Kukko, A., Jaakkola, A., Liang, X., Wang, Y., Hyyppä, H., Katoh, M., 2015. Comparison of laser and stereo optical, SAR and InSAR point clouds from air- and space-borne sources in the retrieval of forest inventory attributes. Remote Sens. 7, 15933–15954.